Information Sciences 273 (2014) 304–318

Contents lists available at ScienceDirect

Information Sciences

journal homepage: www.elsevier.com/locate/ins

A novel hybrid approach for wind speed prediction

Jujie Wang [a,b,c], Wenyu Zhang [a,*], Jianzhou Wang [d], Tingting Han [a], Lingbin Kong [a]

[a] Key Laboratory for Semi-Arid Climate Change of the Ministry of Education, College of Atmospheric Sciences, Lanzhou University, Lanzhou 730000, China
[b] College of Science, Nanjing University of Posts and Telecommunications, Nanjing 210046, China
[c] Key Laboratory for Land Surface Process and Climate Change in Cold and Arid Regions, Chinese Academy of Sciences, Lanzhou 730000, China
[d] School of Mathematics and Statistics, Lanzhou University, Lanzhou 730000, China

ARTICLE INFO

Article history:
Received 8 February 2012
Received in revised form 25 February 2014
Accepted 28 February 2014
Available online 13 March 2014

Keywords:
Wind speed prediction
Seasonal adjustment
Exponential smoothing
Neural network
Hybrid approach

ABSTRACT

It is important to improve the accuracy of wind speed predictions for wind park management and for conversion of wind power to electricity. However, due to the chaotic and intrinsic complexity of weather parameters, the prediction of wind speed data using different patterns is difficult. A hybrid model known as SAM–ESM–RBFN is proposed for capturing these different patterns and obtaining better prediction performance. This model is based on the seasonal adjustment method (SAM), exponential smoothing method (ESM), and radial basis function neural network (RBFN). The mean hourly wind speed data from two meteorological stations in the Hexi Corridor of China were used as examples to evaluate the performance of the proposed approach. To avoid randomness due to the RBFN model or the RBFN component of the hybrid model, all of the simulations were repeated 30 times prior to averaging. The SAM–ESM–RBFN model numerically outperformed the following models: the Holt–Winters model (HWM), the multilayer perceptron neural network (MLP), the ESM, the RBFN, the hybrid SAM and ESM (SAM–ESM), the hybrid SAM and RBFN (SAM–RBFN), and the hybrid ESM and RBFN (ESM–RBFN). Overall, the proposed approach was effective in improving the prediction accuracy.

1. Introduction

Special attention has been focused on renewable energy due to environmental deterioration and conventional resource depletion. Wind power is a clean and non-polluting renewable energy source. Recently, the amount of energy generated by wind power has rapidly increased. The installed wind power capacity increased by nearly 200% between 2005 and 2009 [62]. In 2009, 340 TW h of wind energy was generated worldwide, which accounted for 2% of electricity usage worldwide. In addition, the capacity of wind-powered generators reached 159.2 GW in 2009. The amount of energy produced from wind sources has doubled over the last 3 years and is expected to increase in the future [14].

However, many problems have occurred with the rapid development of wind power. One of the main problems associated with generation of wind power is the continuous fluctuation of wind speed. Fluctuating wind speeds make it difficult to predict how much power will be injected into a distribution network, which can result in energy transportation issues [47]. Thus, improving the accuracy of wind power prediction is highly important. It is widely accepted that wind power prediction should be based on actual wind signal forecasts rather than on the output power of wind turbines [19]. Thus, obtaining accurate wind speed predictions has become increasingly important.

* Corresponding author. Tel.: +86 931 8911031; fax: +86 931 8914278.
E-mail address: zhangwy@lzu.edu.cn (W. Zhang).

http://dx.doi.org/10.1016/j.ins.2014.02.159
0020-0255/

Generally, wind speed predictions can be classified into two categories: short-term predictions (time scales of minutes, hours, and days) and long-term predictions (time scales of months and years). For short-term predictions, accurate predictions are important in minimizing scheduling errors, which impact grid reliability and market-based ancillary service costs [27]. For long-term predictions, prediction accuracy is important for site selection, performance prediction, windmill planning, and selection of the optimal wind machine size for a particular site [36]. The focus of this study was on short-term wind speed prediction.

Many prediction methods have been developed over the last two decades. These methods can be divided into two categories: statistical models and machine-learning models. Statistical models primarily use a time series approach and have been successfully applied for forecasting [14,27,44,49]. These models are based on the assumption that a linear correlation structure exists among time series values. Therefore, non-linear patterns cannot be captured using these models. To overcome this limitation, machine-learning models (which primarily include artificial neural networks (ANN), support vector machines, and fuzzy logic methods), have been used to improve non-linear time series predictions [9,12,17,21,22,26,30,31,34,38,50,53,55,57].

Wind is a weather-driven renewable resource that depends on climate. The two most commonly encountered phenomena in wind speed series are seasonal variations and trend variations [27]. However, seasonal variations are often neglected in wind speed series predictions, and the large seasonal variations result in large prediction deviations. According to Zhang and Qi [60], de-seasonalization can dramatically reduce the prediction errors in seasonal time series. The seasonal adjustment method (SAM) was used to decompose the time series into seasonal and trend components as well as to simulate and predict the seasonal component. Thus, the SAM was used to pre-process raw wind speed data in this study. Beyond the seasonal component of the wind speed series, the trend component is complex and contains linear and non-linear characteristics. Thus, the sole use of a statistical model or a machine-learning model cannot adequately forecast the wind speed if a time series contains linear and non-linear patterns, and accordingly, no single method or model can work well in all situations [8,61]. Generally, it is more effective to combine different models that use different sources of information [25,41,52]. Hybrid models have been rapidly developed to improve prediction accuracy [1,4,10,11,15,16,37,48,56]. For example, Monfared et al. proposed a new strategy for wind speed prediction that was based on fuzzy logic and artificial neural networks [37]. In addition, Fan and Liu combined a gray-related and weighted combination with the revised parameter method to predict wind speed [15]. Ata and Kocyigit applied an adaptive neuro-fuzzy inference system (ANFIS) model to predict the tip speed ratio (TSR) and the power factor of a wind turbine [1]. Furthermore, Sancho et al. discussed the application of the complete evolutionary support vector machines algorithm to real wind speed prediction problems for Spanish wind farm turbines [48].

As one of the most popular statistical models, the main advantage of exponential smoothing methods (ESM) is their robustness, which allows for fast and efficient implementation with descriptive and inferential statistics [18]. The ESM has been studied extensively for linear identification and time series prediction. However, the ESM is rarely used for wind speed prediction [33]. Artificial neural networks are useful for predicting wind speeds because they are able to capture subtle functional relationships from empirical data if the underlying relationships are unknown or are difficult to describe. Radial basis function neural networks (RBFN) are special neural networks that have been studied extensively by researchers for non-linear identification and time series prediction. A RBFN can rapidly learn complex patterns and tendencies that occur in data. In addition, RBFN can arbitrarily approximate any multivariate continuous function in a compact domain if a sufficient number of radial basis function units are provided [42,45]. Thus, ESM and RBFN were used to predict wind speeds in this study.

Due to the chaotic and intrinsic complexity of weather parameters, it is difficult to predict wind speed data or wind patterns. In this study, a hybrid model (referred to as SAM–ESM–RBFN) for wind speed prediction based on the SAM, ESM, and RBFN was proposed to capture different patterns and improve prediction performance. First, the SAM was used to eliminate the seasonal components from raw wind speed data and to predict the seasonal component. Next, the ESM and RBFN were used to capture the linear and non-linear patterns, which were used to predict the wind speed trends. Third, the predicted trend was adjusted by combining the seasonal index with the predicted trend function. Finally, the mean hourly wind speed data from the two meteorological stations in the Hexi Corridor of China were used as illustrative examples to evaluate the performance of the SAM–ESM–RBFN model. In addition, the HWM is a popular double exponential smoothing method that includes seasonal and trend components. The multilayer perceptron neural network (MLP) has often been used to predict time series. To evaluate the performance of the proposed approach, the SAM–ESM–RBFN model was compared with the HWM, MLP, ESM, RBFN, SAM and ESM (SAM–ESM) models, the hybrid SAM and RBFN (SAM–RBFN) model, and the hybrid ESM and RBFN (ESM–RBFN) model. The numerical results indicate that the proposed method outperforms these models. Thus, the proposed method is effective in improving the accuracy of wind speed predictions. The remainder of this study is organized as follows. Section 2 presents the SAM–ESM–RBFN approach for short-term wind speed prediction. Section 3 discusses the different error criteria used to evaluate the prediction accuracy. Section 4 presents the numerical results obtained from two real datasets, and the conclusions are presented in Section 5.

2. Proposed approach

This section presents the SAM–ESM–RBFN method. First, the SAM, ESM, and RBFN are briefly introduced, and the approach of the SAM–ESM–RBFN model is presented.

2.1. Seasonal adjustment methods (SAM)

Seasonal and trend components coexist in wind speed series. Generally, two operations are used to generate composite models with seasonal and trend components: addition and multiplication. According to Zhang and Qi [60], the classical multiplicative decomposition model is appropriate for many time series that are characterized by increasing seasonal variations. However, if the seasonal variation is relatively consistent with the trend, the additive decomposition model should be used. In addressing real problems, it is difficult to determine which model is more suitable [20]. Thus, both multiplicative and additive decomposition models [39] were used in this study to forecast wind speed.

Throughout this study, T, m, l are given as integers and $T = l \times m$. In addition, α denotes the wind speed at time α, $t \in \{1, 2, \ldots, T\}$, and I_t and p_t represent the seasonal and trend components, respectively.

The multiplicative wind speed x_t at time t can be expressed as

$$x_t = p_t \times I_t. \tag{1}$$

Thus, the seasonal index I_t can be obtained as follows:

$$I_t = x_t / p_t. \tag{2}$$

Next, the data $\{x_t\}$, $t \in \{1, 2, \ldots, T\}$ were divided into l groups, with each group representing one cycle. Next, m data were used in each cycle because $T = l \times m$. In addition, $\{x_t\}$, $t \in \{1, 2, \ldots, T\}$ is denoted as $x_{11}, x_{12}, \ldots, x_{1s}, \ldots, x_{1m}, x_{21}, x_{22}, \ldots, x_{2s}, \ldots, x_{2m}, \ldots, x_{k1}, x_{k2}, \ldots, x_{ks}, \ldots, x_{km}, \ldots, x_{l1}, x_{l2}, \ldots, x_{ls}, \ldots, x_{lm}$ ($k = 1, 2, \ldots, l$; $s = 1, 2, \ldots, m$), where x_{ks} represents the s-th datum of the k-th cycle.

The average of each cycle was used to approximate the unknown trend component [20]. The average of the k-th cycle was derived as follows:

$$\bar{x}_k = (x_{k1} + x_{k2} + \cdots x_{km})/m \quad (k = 1, 2, \ldots, l). \tag{3}$$

If I_{ks} represents the normalization data for items x_{ks}, then

$$I_{ks} = \frac{x_{ks}}{\bar{x}_k} \quad (k = 1, 2, \ldots, l;\ s = 1, 2, \ldots, m). \tag{4}$$

In addition, I_s was defined as follows:

$$I_s = \frac{I_{1s} + I_{2s} + \cdots I_{ls}}{l} \quad (s = 1, 2, \ldots, m). \tag{5}$$

This definition of I_s confirms the normalization process and is expressed as follows:

$$\sum_{s=1}^{l} I_s = \frac{1}{l}\sum_{k=1}^{l}\sum_{s=1}^{m} I_{ks} = \frac{1}{l}\sum_{k=1}^{l}\left(\sum_{s=1}^{m} x_{ks}/\bar{x}_k\right) = \frac{1}{l}\sum_{k=1}^{l} l = l.$$

Using I_s, the series without any seasonal component was obtained as follows:

$$x'_{ks} = \frac{x_{ks}}{I_s} \quad (s = 1, 2, \ldots, m;\ k = 1, 2, \ldots, l). \tag{6}$$

The new data series can be obtained without the seasonal component if the data items $x'_{11}, x'_{12}, \ldots, x'_{1l}; \ldots$, and $x'_{m1}, x_{m2}, \ldots, x'_{ml}$ are re-recorded back to $x'_1, x'_2, \ldots, x'_T$.

Similar to the multiplicative decomposition model, for the additive decomposition model, the following equations were required to replace Eqs. (1), (2), (4), and (6), respectively:

$$x_t = p_t + I_t, \tag{1'}$$

$$I_t = x_t - p_t, \tag{2'}$$

$$I_{ks} = x_{ks} - \bar{x}_k \quad (k = 1, 2, \ldots, l;\ s = 1, 2, \ldots, m), \tag{4'}$$

$$x'_{ks} = x_{ks} - I_s \quad (k = 1, 2, \ldots, l;\ s = 1, 2, \ldots, m). \tag{6'}$$

A cycle length of $m = 24$ was considered based on the influence of the wind speed data.

2.2. Exponential smoothing methods (ESM)

The ESM can be applied to time series forecasting. The ESM is commonly applied to financial market and economic data but can be used with any discrete set of repeated measurements [5,18,35,40]. The raw data sequence is represented by $\{x_t\}$, and the ESM output is represented by $\{s_t\}$. For a sequence of observations that begins at time $t = 0$, the simplest form of the ESM is given as follows:

$$\begin{aligned} s_1 &= x_0, \\ s_t &= \alpha x_{t-1} + (1-\alpha)s_{t-1}, \end{aligned} \tag{7}$$

where α is the smoothing factor, and $0 < \alpha < 1$. If α is near 1, the smoothing effect is lower, and additional weight is given to the recent changes in the data. However, if α is near 0, the smoothing effect is greater, and fewer responses to recent changes are observed [6]. No formally correct procedure exists for choosing α. Occasionally, the statistician's judgment is used to choose an appropriate factor.

The following equation was obtained by substituting the defining equation for the simple ESM back into itself:

$$\begin{aligned} s_t &= \alpha x_{t-1} + (1-\alpha)s_{t-1} = \alpha x_{t-1} + \alpha(1-\alpha)x_{t-2} + (1-\alpha)^2 s_{t-2} \\ &= \alpha[x_{t-1} + (1-\alpha)x_{t-2} + (1-\alpha)^2 x_{t-3} + (1-\alpha)^3 x_{t-4} + \cdots + (1-\alpha)^{t-2}x_1] + (1-\alpha)^{t-1}x_0. \end{aligned} \tag{8}$$

The smoothed statistic s_t becomes the weighted average of the past observations. In addition, the weights assigned to the previous observations are generally proportional to the geometric progression terms $\{1, (1-\alpha), (1-\alpha)^2, (1-\alpha)^3, \ldots\}$. The prediction value of the ESM is a weighted combination of the current and historical values. In this case, the ESM is a linear method.

The multi-step prediction method was used in this study. The multi-step prediction (predicting more than 1 h in advance) process was iterative. Thus, the outputs of the system were re-entered as inputs. In this case, the previous prediction data were used rather than the true values to predict the subsequent values if no previous true values existed [7]. By considering the exponentially decreasing ESM weights and the cycle impacts of real wind speed, the data at time t were predicted using data from the 24 h before time t. Next, the following corresponding equation was used:

$$s_t = \alpha[x_{t-1} + (1-\alpha)x_{t-2} + (1-\alpha)^2 x_{t-3} + (1-\alpha)^3 x_{t-4} + \cdots + (1-\alpha)^{23}x_{t-24}] \quad (t = 25, 26, \ldots, T). \tag{9}$$

The forecasting data for time t were subsequently used in the same process rather than the true values to predict the time $t+1$. In addition, the optimum α value was determined experimentally (see Section 4.3.1).

2.3. Radial basis function neural networks (RBFN)

The RBFN is generally composed of three layers, including the input, hidden, and output layers [3,54]. The input layer feeds the input data for each of the nodes in the hidden layer. The hidden layer is different from the other neural networks because each of its nodes represents a data cluster that is centered at a particular point with a given radius. Each node in the hidden layer is used to calculate the distance from the input vector to its own center. The calculated distance is transformed using a basis function (i.e., the Gaussian function) to obtain an output from each node. The output from the node is multiplied by a constant or weighting value before feeding it into the output layer. The output layer consists of only one node, which is used to sum the outputs of the hidden layer to yield a final output value [28,59]. A generic RBFN architecture with an input m and hidden nodes N is illustrated in Fig. 1.

The output of the RBFN is described by the following equation:

$$y = f(x) = \sum_{k=1}^{N} w_k \phi_k(\|x - c(k)\|, \sigma_k), \tag{10}$$

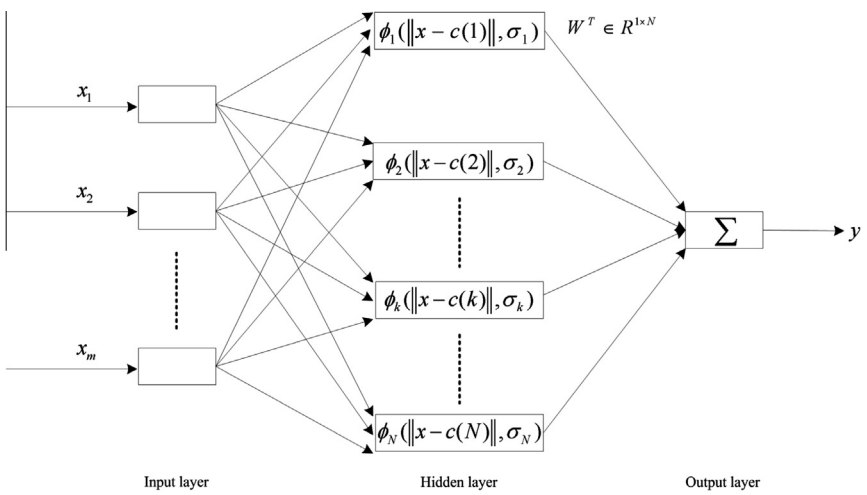

Fig. 1. General structure of the RBFN.

where y is the actual network output, $x \in R^{m\times 1}$ is an input vector signal (with individual vector components of x_j for $j = 1, 2, \ldots, m$, and $x = [x_1, x_2, \ldots, x_m]^T \in R^{m\times 1}$). In addition, $W = [w_1, w_2, \ldots, w_N]^T \in R^{N\times 1}$ is the vector of the weights in the output layer, N is the number of neurons in the hidden layer, and $\phi_k(\cdot)$ is the basis function of the network from R^+ to R. Furthermore, $c(k) = [c_{k1}, c_{k2}, \ldots, c_{km}]^T \in R^{m\times 1}$ is the center vector of the k-th node, σ_k is the bandwidth of the basis function $\phi_k(\cdot)$, and $\|\cdot\|$ denotes the Euclidean distance [29]. During the training procedure, the steepest gradient descent learning process is used to adjust the appropriate parameter settings. This process is used to optimize the network mapping performance.

During the RBFN design process, it is difficult to determine the number of the nodes in the hidden layer. If an insufficient number of nodes are selected, the performance of the network is limited. Conversely, the selection of a sufficient number of nodes results in a large network and greater over-fitting of the network process. To overcome this problem, a network growing and pruning algorithm based on the significance of a neuron was adopted. The significance was defined as a neuron's statistical contribution to the overall performance of a network. A new neuron was only added if its significance was greater than the chosen threshold. Conversely, neurons were pruned if their significance was less than the chosen threshold. The network growing and pruning algorithm is described below [23,29].

(1) *Pruning node:* To define the significance of a neuron for pruning (SNP), it was assumed that the RBFN output for N neurons and an input of x is given by Eq. (10). If the neuron q is removed, the following RBFN output is obtained for the remaining $N-1$ neurons:

$$y_q = \sum_{k=1}^{q-1} w_k \phi_k(\|x - c(k)\|, \sigma_k) + \sum_{k=q+1}^{N} w_k \phi_k(\|x - c(k)\|, \sigma_k). \tag{11}$$

Therefore, for an input of $x(i)$, the error resulting from removing a neuron q was defined as the absolute difference between y and y_q.

$$PErr(i, q) = |y - y_q| = |w_q| \phi_q(\|x(i) - c(q)\|, \sigma_q). \tag{12}$$

The significance of a neuron for pruning was defined as the average error for all M sequentially learned inputs that resulted from removing a neuron q.

$$\mathrm{SNP}(q) = \frac{\sum_{i=1}^{M} PErr(i, q)}{M} = \frac{|w_q|}{M} \sum_{i=1}^{M} \phi_q(\|x(i) - c(q)\|, \sigma_q). \tag{13}$$

If $\mathrm{SNP}(q) < TPErr$ (a predefined threshold value), the neuron q does not significantly contribute to the overall performance of the network. Thus, this neuron should be removed.

(2) *Growing node:* The definition of the significance of a neuron for the node growing process was similar to the definition of significance used for pruning. For the newly added neuron $N+1$, the output of the RBFN with $N+1$ neurons was

$$y_{N+1} = \sum_{k=1}^{N+1} w_k \phi_k(\|x - c(k)\|, \sigma_k). \tag{14}$$

Therefore, for a given input of $x(i)$, the error produced from the newly added neuron $N+1$ was defined as the absolute difference between y and y_{N+1}.

$$GErr(i, N+1) = |y - y_{N+1}| = |w_{N+1}| \phi_{N+1}(\|x(i) - c(N+1)\|, \sigma_{N+1}). \tag{15}$$

The significance of a neuron for growing (SNG) was defined as the average error for all M sequentially learned inputs following the addition of $N+1$ neurons.

$$\mathrm{SNG}(N+1) = \frac{\sum_{i=1}^{M} GErr(i, N+1)}{M} = \frac{|w_{N+1}|}{M} \sum_{i=1}^{M} \phi_{N+1}(\|x(i) - c(N+1)\|, \sigma_{N+1}). \tag{16}$$

The parameters associated with the new $N+1$ neuron were treated as follows:

$$\begin{aligned} w_{N+1} &= -\mathrm{RMSE} \Big/ \sum_{i=1}^{M} \phi_{N+1}(\|x(i) - c(N+1)\|, \sigma_{N+1}), \\ c(N+1) &= \{x(i) | i = \arg\max(|d(i) - y(i)|)\}, \\ \sigma_{N+1} &= k\|x(i) - c_{nr}\|, \end{aligned} \tag{17}$$

where c_{nr} is the center nearest $x(i)$, and k is a real number ($k = 0.95$ in this study). In addition, $d(i)$ and $y(i)$ represent the actual and predicted values at time i, respectively.

If $\mathrm{SNG}(N+1) > TGErr$ (a predefined threshold value), the $N+1$ neuron significantly contributes to the overall performance of the network. Thus, this new neuron should be added to the network.

A three-layer RBFN was used in this study (with the Gaussian function as the non-linear basis function). In addition, the size of the RBF layer was determined by a network growing and pruning algorithm that prevented over-fitting of the RBFN. Two neurons in the hidden layer were provided at the beginning of the training process. Next, the corresponding centers were uniformly assigned from the data range. The initial weights were randomly selected and were between −0.5 and 0.5. The following parameters were set: *TPErr* = 0.02 and *TGErr* = 0.0003. In addition, the input data were normalized between 0 and 1.

2.4. Proposed approach

The proposed SAM–ESM–RBFN approach for predicting short-term wind speed was based on a combination of SAM, ESM, and RBFN methods. First, the SAM was used to separate the wind speed series into seasonal and trend components and to simulate and predict the seasonal component. Next, the ESM and RBFN were used to capture the linear and non-linear patterns and were used to predict the trend components of the wind speed series. Finally, the prediction value of the raw wind speed series was calculated by combining the seasonal index with the predicted trend component function. The algorithm used in this study is described below and is illustrated in Fig. 2.

Step 1: Remove the seasonal component. In this step, the wind speed series were decomposed into seasonal and trend components by the SAM. In addition, the seasonal indices were calculated.

Step 2: Capture the linear pattern. The ESM was primarily used to capture the linear pattern from the trend component of the wind speed series.

Step 3: Capture the non-linear pattern. The RBFN was primarily used to capture the non-linear pattern from the trend component of the wind speed series. The RBFN was constructed from the error between the trend component and its predicted value from the ESM.

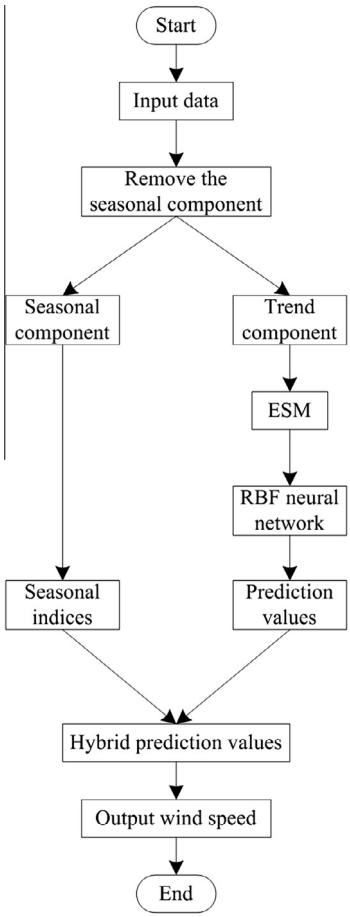

Fig. 2. Flow chart for the proposed hybrid method.

Step 4: Adjust the trend component. The prediction value of the trend component was adjusted by adding the predicted value of the residual error series to the predicted value of the ESM trend component.

Step 5: Predict the raw wind speed series. The prediction values of the raw wind speed data series were calculated by combining the seasonal index with the predicted trend component value.

3. Evaluation criteria

To identify the best model quantitatively, two criteria were used to evaluate and compare the models. These criteria included the root mean-square error (RMSE) and the mean absolute percentage error (MAPE).

$$\mathrm{RMSE} = \left(\frac{1}{T}\sum_{t=1}^{T} e_t^2\right)^{1/2}, \tag{18}$$

$$\mathrm{MAPE} = \frac{1}{T}\sum_{t=1}^{T}\left|\frac{e_t}{x_t}\right|, \tag{19}$$

where $e_t = x_t - f_t$, and T corresponds to the sample size. In addition, x_t and f_t represent the actual and predicted values at time t, respectively. Currently, the wind speed forecasted by the MAPE ranges from 25% to 40%. These wind speed predictions depend on the forecasting methods, forecasting horizon, and wind speed characteristics at a given location. In general, the shorter forecasting horizons correspond to more stable wind speed variations and smaller forecasting errors. Otherwise, the forecasting error will increase [58].

4. Experimental design and comparison results

The performance of the SAM–ESM–RBFN was verified by applying it to a non-linear dynamic system for predicting wind speed. The performance of the algorithm was evaluated by comparing these results with the results obtained from similar models. All of the simulations were programmed with MATLAB version 7.8 and SPSS version 16.0. In addition, the original data were scaled to a range of 0–1.0 for building the RBFN prediction model.

4.1. Data sets

The Hexi Corridor of China has abundant wind resources due to its geographical characteristics. The Jiuquan and Guazhou regions, which are located in the Hexi Corridor of China, are potentially valuable wind farm sites. The following advantages result from wind energy development: (i) greater wind power density, (ii) longer periods of valid wind power generation, (iii) climatic conditions that benefit and prolong the life of wind turbines, and (iv) low investment costs for construction. In this study, the mean hourly wind speed data in Jiuquan and Guazhou were used as an illustrative example to evaluate the performance of the proposed approach.

To validate the developed model, the first 696 values used were obtained from the training sample, and the remaining 48 values were used for each of the two model evaluation sites. Figs. 3 and 4 show the hourly wind speed data from the two sites.

4.2. De-seasonalization process

The multiplicative and additive decomposition models were used in two case studies to eliminate the seasonal components of the raw wind speed datasets. Because the additive and multiplicative decomposition models are similar, this study focused on the multiplication model. The calculation results of the hybrid models, which were based on the additive decomposition process, are shown in Table 3. Figs. 5 and 6 depict the multiplicative decomposition processes of the raw wind speed datasets in Jiuquan and Guazhou. Each wind speed series was separated into seasonal and trend components (Figs. 5 and 6).

4.3. Prediction results of the trend component

The trend components of the raw wind speed series were predicted in this section. First, the ESM was used to capture the linear patterns of the trend components. Next, the RBFN was used to capture the non-linear patterns of the trend components and was constructed from the residual error series after the ESM simulation. This process is described below.

4.3.1. ESM prediction of the trend component

Corresponding to the previous observations, the ESM depends on the selection of α. In this study, the optimal α value was determined based on the data. The previous 24 data points were used as input data by considering the cycle effects of the wind speed data. Next, the data were fed to the model as outputs. Meanwhile, 696 training data points were divided into 672 sample pairs. The corresponding data format is defined in Fig. 7. In Fig. 7, $tr_t (t = 1, 2, \ldots, 696)$ represents the actual trend

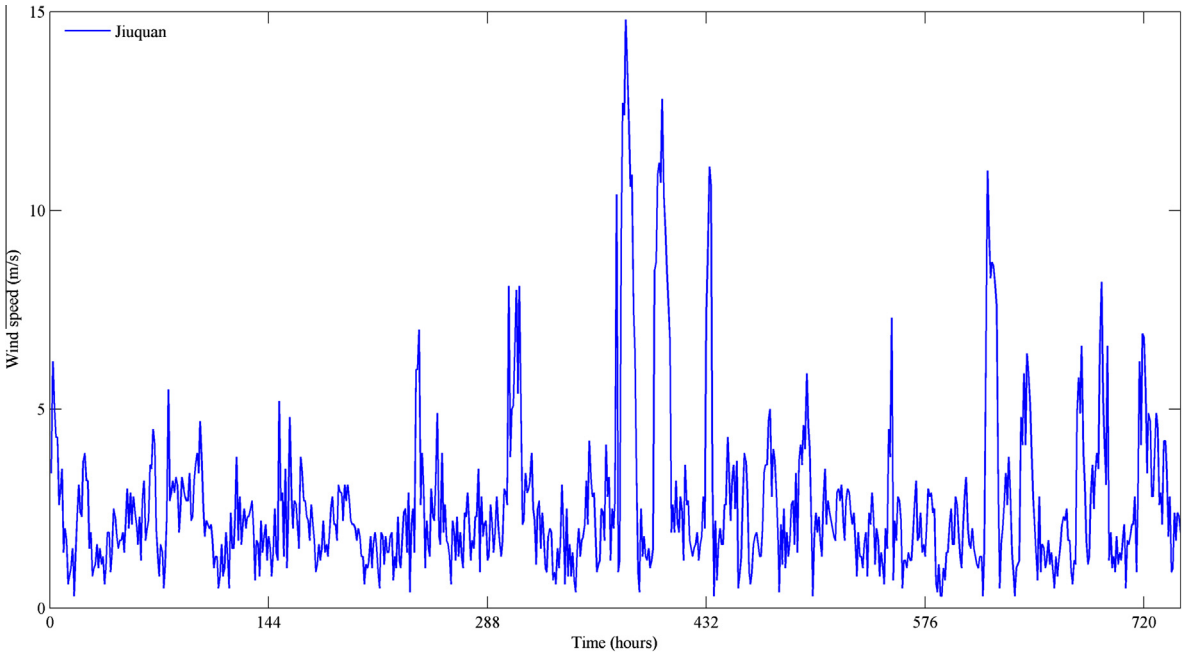

Fig. 3. Mean hourly wind speed data from the Jiuquan region.

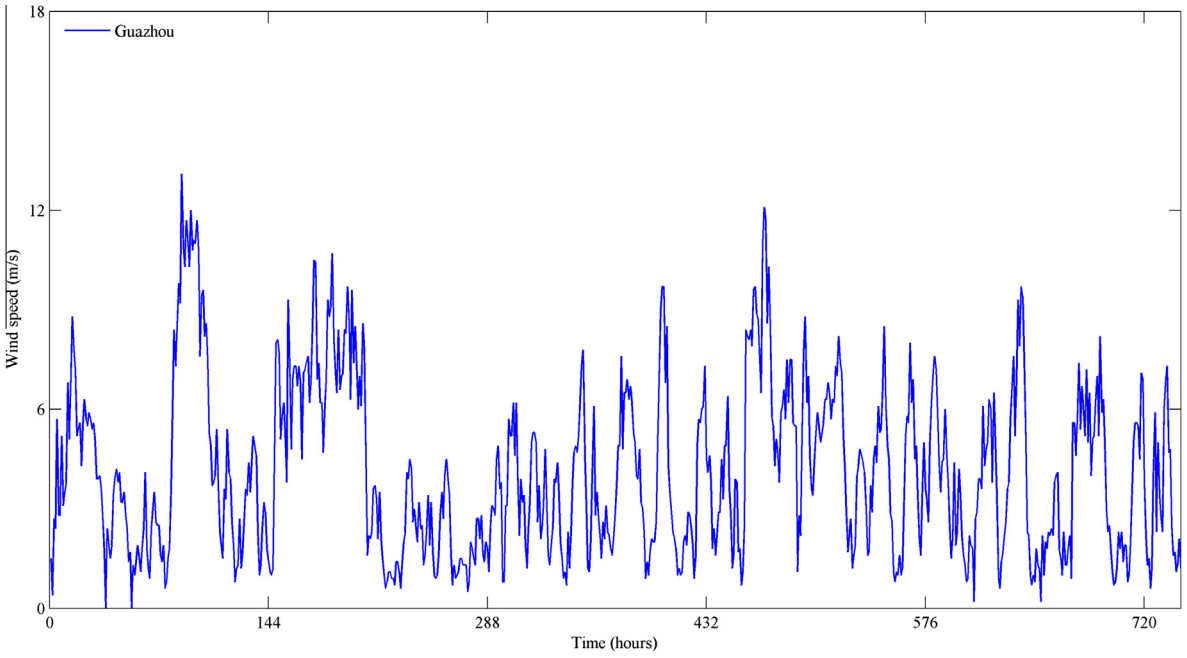

Fig. 4. Mean hourly wind speed data from the Guazhou region.

component value at time t. When different α values were used (changing the α value from 0.1 to 0.9 in Eq. (9)), the values of the fitting sequence were calculated from the 672 sample pairs. Due to two evaluation criteria errors, the smallest error was the model error, and the corresponding α value was the optimal α value. Table 1 displays the statistical error measures. Based on these results, $\alpha = 0.8$ minimized the trend component measurement errors in Jiuquan, and $\alpha = 0.9$ minimized the trend component measurement errors in Guazhou. Next, multi-step forecasting was applied. The 48 predictive values were obtained by 16 iterations of the prediction process. In each prediction process, three predictive values can be obtained in the iterative process. For example, through three steps of forecasting, the 697th–699th can be predicted by the

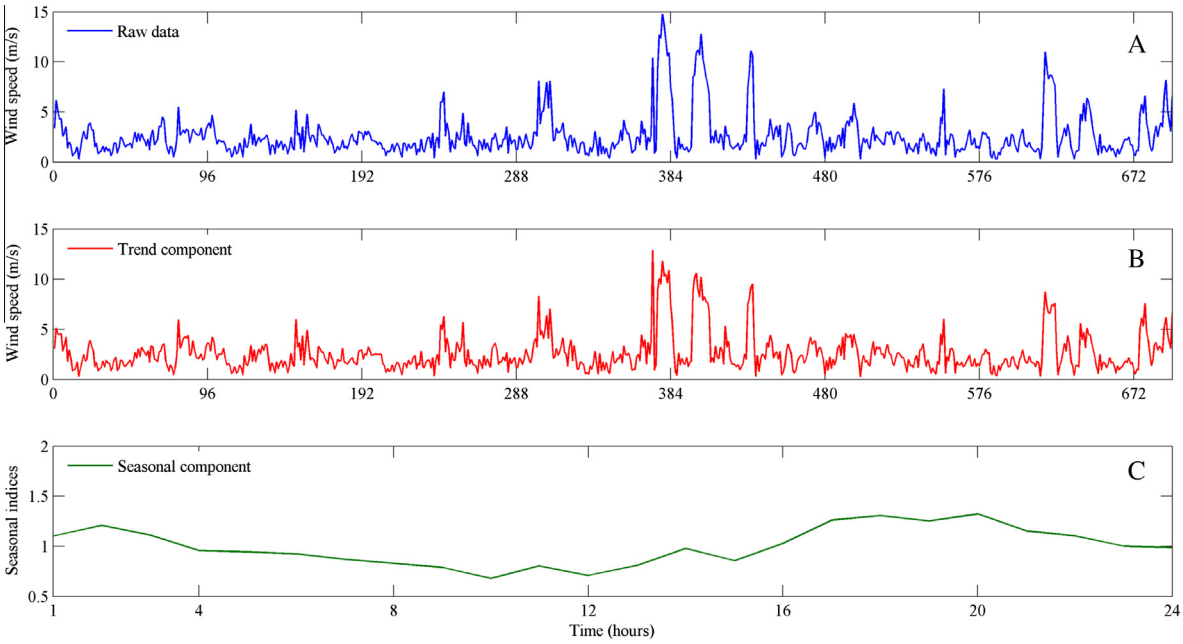

Fig. 5. De-seasonalization process for the raw wind speed series in Jiuquan: (A) raw wind speed series, (B) trend component of the raw wind speed series, and (C) seasonal component of the raw wind speed series.

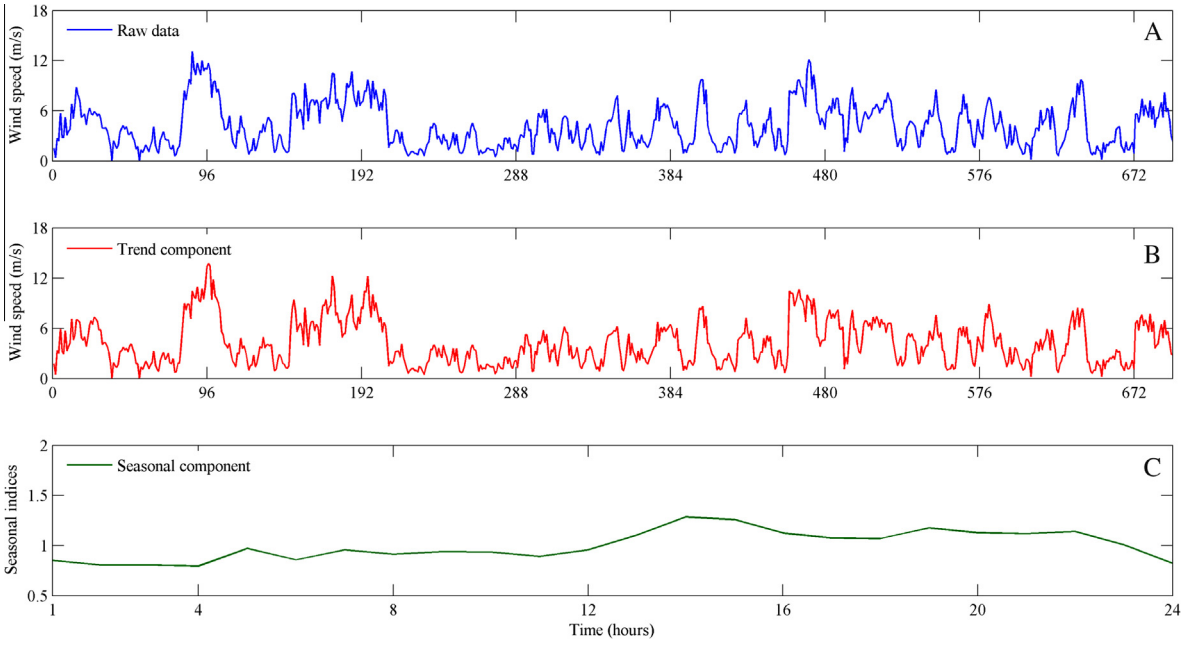

Fig. 6. De-seasonalization process for the raw wind speed series in Guazhou: (A) raw wind speed series, (B) trend component of the raw wind speed series, and (C) seasonal component of the raw wind speed series.

673rd–696th. In the same way, the 700th–702nd also can be predicted by the 676th–699th, and so on. Thus, the 48 predictive values can be obtained. Fig. 7 shows one time prediction process in the forecasting period.

4.3.2. Error correction of the trend components by the RBFN

The RBFN was used for error correction to improve the prediction accuracy of the ESM. The RBFN was constructed based on the error between the trend component and its ESM predicted values. Similar to the ESM procedure, the previous 24 data were fed in as input data, and the next set of data were fed in as output data. In addition, the training data were divided into

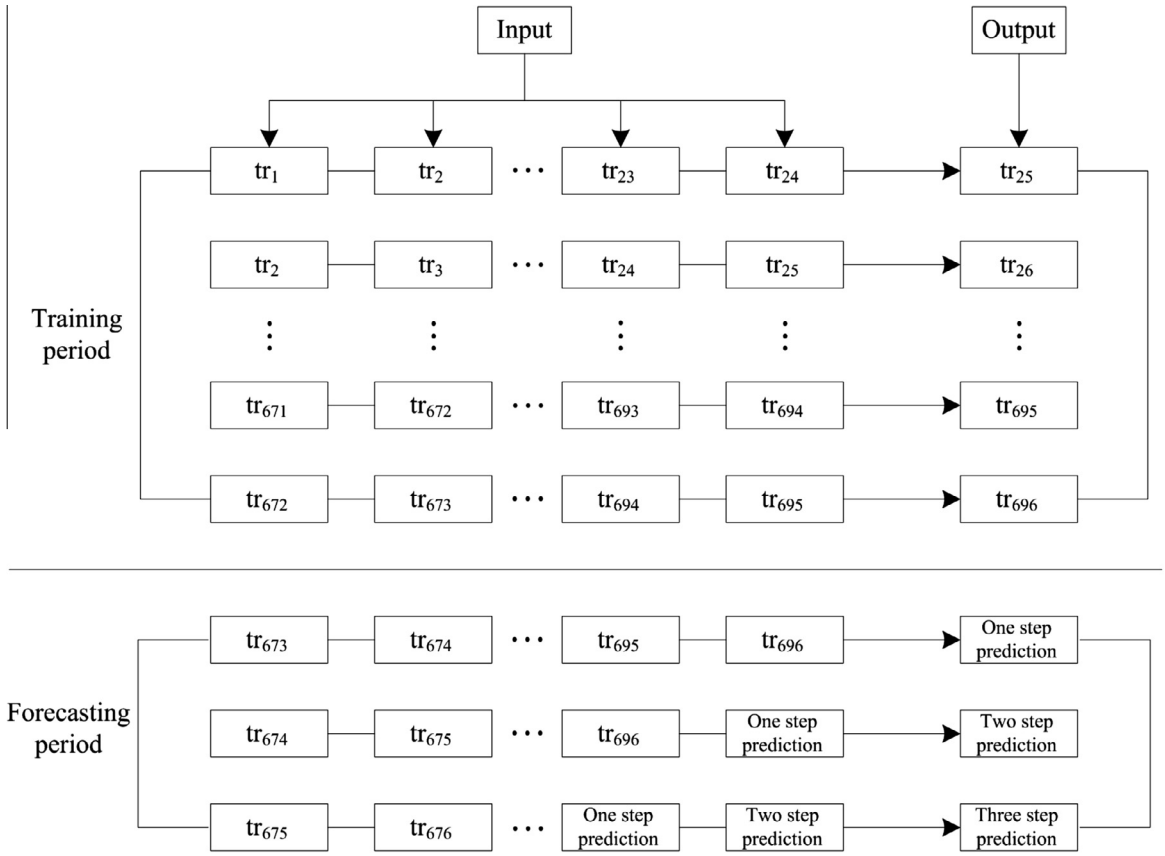

Fig. 7. Data input and output format for the ESM modeling process.

Table 1
Statistical error measurements for the ESM with different α values.

Jiuquan										Guazhou									
Alfa	0.1	0.2	0.3	0.4	0.5	0.6	0.7	0.8	0.9	Alfa	0.1	0.2	0.3	0.4	0.5	0.6	0.7	0.8	0.9
RMSE	1.72	1.59	1.52	1.46	1.33	1.27	1.03	0.96	0.99	RMSE	1.83	1.71	1.65	1.42	1.37	1.21	1.14	1.09	1.04
MAPE	0.91	0.86	0.78	0.72	0.68	0.62	0.53	0.45	0.48	MAPE	0.97	0.92	0.87	0.75	0.64	0.58	0.52	0.49	0.47

648 sample pairs. The corresponding data format is defined in Fig. 8. In Fig. 8, $r_t = tr_t - s_t (t = 25, 26, \ldots, 696)$ represents the residual error at time t, and tr_t and s_t represent the actual trend component and prediction values of the ESM at time t, respectively. Next, the prediction values of the residual error were obtained. Finally, the prediction value of the trend component was adjusted by adding the prediction value of the residual error series to the prediction value of the trend component from the ESM. The prediction comparisons of the trend components with the ESM and ESM–RBFN results are shown in Table 2.

4.4. Raw wind speed series prediction results

The seasonal index and the prediction values of the trend components were calculated in Sections 4.2 and 4.3. The final prediction value of the raw wind speed data was calculated by adjusting the seasonal index to the predicted trend component value from the ESM–RBFN. Figs. 9 and 10 show the prediction results for the two raw wind speed series. Model comparisons are provided in the next section to validate the prediction capacity of the proposed hybrid approach.

4.5. Model comparisons

The popular HWM is a double exponential smoothing method that includes seasonal and trend components. The multilayer perceptron neural network (MLP) is commonly used for time series predictions. Because the hidden layer network is

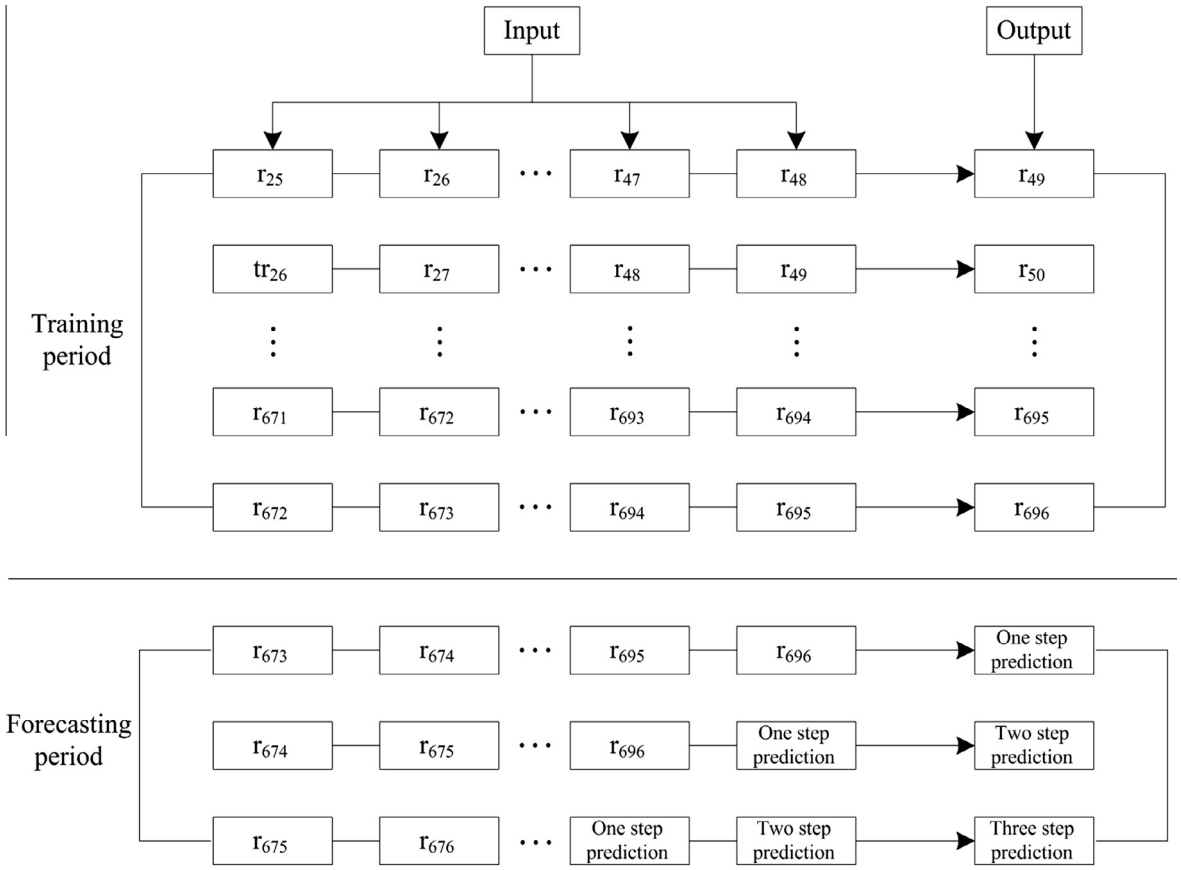

Fig. 8. Input and output data formatting for the RBFN modeling process.

Table 2
Prediction comparisons of the trend components with the ESM and ESM–RBFN.

Data	ESM		ESM–RBFN	
	RMSE	MAPE	RMSE	MAPE
Jiuquan	1.12	0.43	0.32	0.12
Guazhou	1.29	0.40	0.42	0.15

sufficient for modeling any complex system with the desired accuracy, the three-layer feed-forward network with one hidden layer (in which the neurons in the input layer have no transfer function) was used in the MLP with logsig or purelin in the hidden layer and output layer as an activation function. In contrast, according to the Kolmogorov theorem, a hidden layer of $2n + 1$ nodes is sufficient for mapping any function to n inputs [43]. Thus, the numbers of nodes in the hidden layer were initially chosen based on the Kolmogorov theorem. The numerical simulation method was used to determine the number of nodes in the hidden layer in the MLP. The numerical simulation results indicated that 49 hidden nodes were optimal. Therefore, a three-layer back propagation neural network with a 24-neuron input layer, a 49-neuron hidden layer, and a 1-neuron output layer was used in this study.

To evaluate the performance of the proposed approach, the SAM–ESM–RBFN was compared with the HWM, MLP, ESM, RBFN, SAM–ESM, SAM–RBFN and ESM–RBFN approaches. The comparison results in Table 3 indicate that the proposed approach has the lowest RMSE and MAPE. These results are explained as follows. First, the SAM–ESM–RBFN approach had a greater prediction capacity relative to the MLP, ESM, and RBFN approach. This result indicates that the SAM–ESM–RBFN approach fully uses each individual model to obtain different information. In addition, the HWM, SAM–ESM, SAM–RBFN, and ESM–RBFN approaches often neglect seasonal component information or use a single model. In contrast, the SAM–ESM–RBFN approach considers all seasonal information patterns and all linear and non-linear structures. Conversely, this finding indicates that the SAM–ESM–RBFN approach also considers the seasonal component and captures different relationships between the wind speed time series. Thus, the proposed approach is effective and can improve the prediction performance.

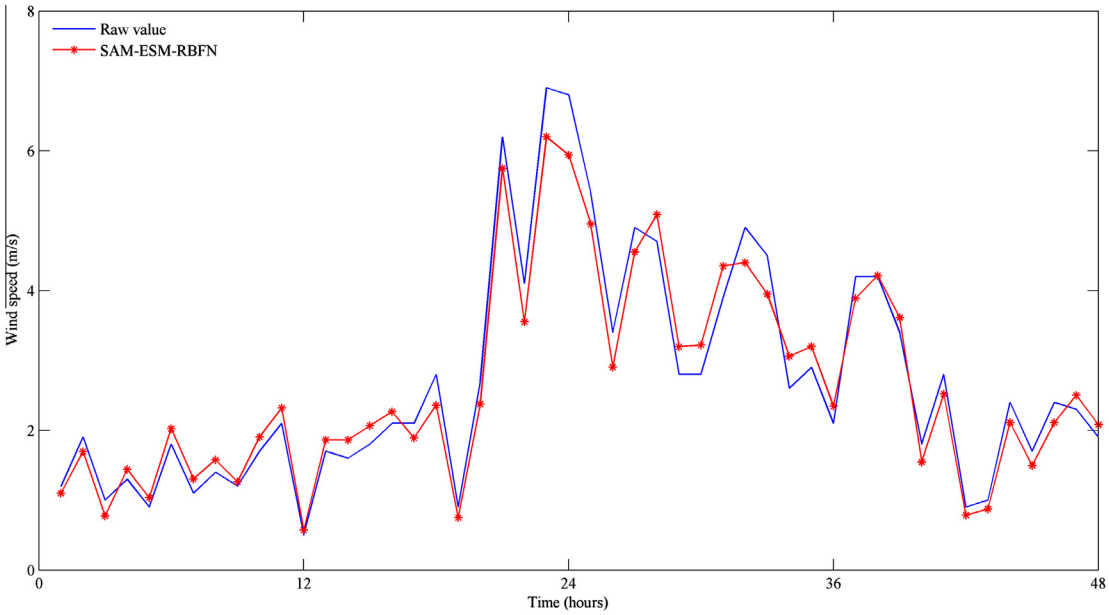

Fig. 9. Prediction results of the raw wind speed time series from the proposed approach in Jiuquan.

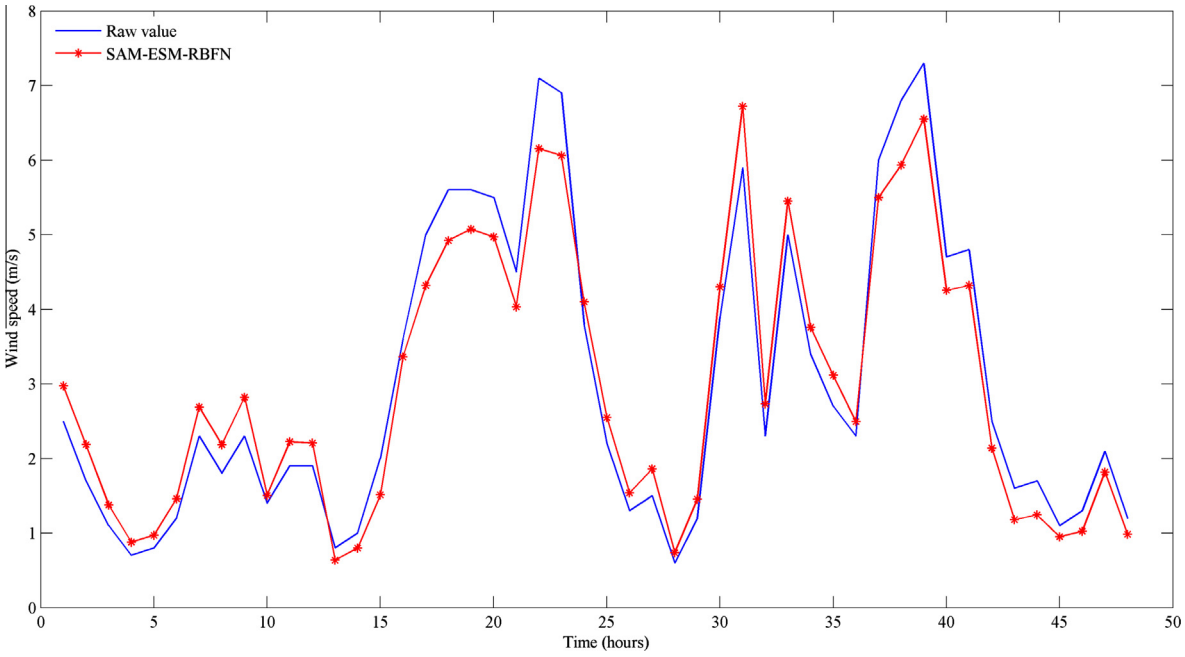

Fig. 10. Prediction results of the raw wind speed time series from the proposed approach in Guazhou.

To verify the calculation efficiency of the proposed prediction approach, the computing time was considered. Different algorithms require different numbers of iterations to obtain similar performance, and the average computing time per iteration is used in every prediction model to compare the different prediction models fairly. Table 4 shows the average computing time per iteration for eight models in two different datasets. Based on these results, the proposed SAM–ESM–RBFN approach has a faster computing ability relative to that of the HWM, SAM–ESM, SAM–RBFN, and ESM–RBFN approaches for two wind speed datasets. However, relative to the MLP, ESM, and RBFNN approaches, the computational speed of the proposed SAM–ESM–RBFN approach was slow. Because this model is a hybrid model, it is slower but more effective. Thus, the SAM–ESM–RBFN approach was acceptable based on its improved prediction accuracy.

Table 3
Error comparison results in eight prediction models.

Data	Seasonal adjustment				
	Models	Errors			
		Multiplicative		Additive	
		RMSE	MAPE	RMSE	MAPE
Jiuquan	HWM	0.79	0.35	–	–
	MLP	1.34	0.47	–	–
	ESM	1.18	0.44	–	–
	RBFN	1.29	0.46	–	–
	SAM–ESM	0.83	0.31	0.94	0.36
	SAM–RBFN	0.78	0.32	0.85	0.39
	ESM–RBFN	0.74	0.28	0.80	0.31
	SAM–ESM–RBFN	0.34	0.12	0.49	0.14
Guazhou	HWM	0.73	0.32	–	–
	MLP	1.60	0.50	–	–
	ESM	1.62	0.48	–	–
	RBFN	1.49	0.50	–	–
	SAM–ESM	0.70	0.27	0.76	0.28
	SAM–RBFN	0.68	0.29	0.73	0.31
	ESM–RBFN	0.66	0.26	0.78	0.30
	SAM–ESM–RBFN	0.45	0.16	0.54	0.18

4.6. Significance test

The Wilcoxon signed-rank test was used to determine if the proposed SAM–ESM–RBFN model was superior to the HWM, MLP, ESM, RBFN, SAM–ESM, SAM–RBFN and ESM–RBFN models for wind speed prediction. The Wilcoxon signed-rank test is a distribution-free and non-parametric technique that can be used to compare two related samples, matched samples, or repeated measurements for a single sample. This test is used to determine whether population means are different and can be used as an alternative to the paired Student's *t*-test, the *t*-test for matched pairs, or the *t*-test for dependent samples. Furthermore, the Wilcoxon signed-rank test has been widely used to evaluate the predictive capabilities of two different models to determine whether they are significantly different [13,24,32,46,51].

Eight prediction sample sets were used for eight different forecasting methods. Seven prediction sample groups were used for the prediction sample sets of the proposed methods for each of the prediction sample sets of the other seven prediction methods. Next, each group prediction sample was subjected to the Wilcoxon signed-rank test and seven comparison tests. To facilitate this discussion, we consider one group of the prediction samples as an example. First, N represents the sample size and the number of pairs. The prediction sample size of each method was 48, and thus, $N = 48$. For $i = 1, 2, \ldots, N$, $y_{1,i}$ and $y_{2,i}$ represent the prediction values of two different methods at time i. If the null hypothesis H_0 is that the median difference between the pairs is zero, the alternative hypothesis H_1 is that the median difference is not zero. The test procedure is described as follows [32,46].

Step 1: For $i = 1, 2, \ldots, N$, calculate the difference $d_i (d_i = y_{2,i} - y_{1,i})$ and $\mathrm{sgn}(y_{2,i} - y_{1,i})$, where sgn is the sign function.
Step 2: Exclude pairs with $d_i = 0$. Let N_r represent the reduced sample size.
Step 3: Rank the remaining $d_i (d_i \neq 0)$ values from smallest to largest by absolute value. Let R_i denote the rank, and affix the sign of each difference to the corresponding rank.
Step 4: Calculate the test statistic $W = \left|\sum_{i=1}^{N_r} [\mathrm{sgn}(y_{2,i} - y_{1,i}) \cdot R_i]\right|$.
Step 5: If N_r is larger than 25, the distribution of W is closely approximated by a normal distribution with a mean of $u_W = \frac{N_r(N_r+1)}{4}$ and a standard error of $\sigma_W = \sqrt{\frac{N_r(N_r+1)(2N_r+1)}{6}}$. Thus, for $N_r \geqslant 25$, the z-statistic can be calculated as follows: $z = \frac{W-0.5}{\sigma_W}$. If $z > z_{critical}$, then reject the H_0. For $N_r < 25$, W is compared with a critical value from a reference table. If $W \geqslant W_{critical,N_r}$, then reject H_0.

Table 4
Average computing time per iteration for eight models in two different datasets.

Data	HWM (s)	MLP (s)	ESM (s)	RBFN (s)	SAM–ESM (s)	SAM–RBFN (s)	ESM-RBF (s)	SAM–ESM–RBFN (s)
Jiuquan	0.73	0.66	0.62	0.63	0.80	0.76	0.79	0.71
Guazhou	0.75	0.67	0.64	0.66	0.78	0.78	0.80	0.74

Table 5
The z-statistic values and p-values of Wilcoxon signed-rank tests between the SAM–ESM–RBFN, and HWM, MLP, ESM, RBFN, SAM–ESM, SAM–RBFN, ESM–RBFN models.

Sites	Models	HWM	MLP	ESM	RBFN	SAM–ESM	SAM–RBFN	ESM–RBFN
Jiuquan	SAM–ESM–RBFN	5.24 (0.00)	8.13 (0.00)	6.36 (0.00)	7.48 (0.00)	4.77 (0.00)	4.16 (0.00)	3.72 (0.00)
Guazhou	SAM–ESM–RBFN	6.45 (0.00)	11.32 (0.00)	10.28 (0.00)	9.61 (0.00)	8.53 (0.00)	7.49 (0.00)	4.37 (0.00)

The numbers in parentheses indicate the corresponding p-values.

We used this test to evaluate the predictive performances of the eight models. Table 5 contains the resulting z-statistic values and p-values from the two-tailed Wilcoxon signed-rank test between the proposed SAM–ESM–RBFN and the individual models, and the numbers in parentheses denote the corresponding p-values. In this study, the significance level is $\alpha = 0.05$, and $z_{critical} = 1.96$. Table 5 shows that each z-statistic value is greater than 1.96, and each p-value is less than 0.05. Therefore, we reject H_0 and decide that the proposed SAM–ESM–RBFN model was significantly different from the other seven models. Because the proposed method can be used to generate the smallest error in the two datasets, we concluded that this method is significantly better for predicting wind speed relative to the other seven models.

5. Conclusions

Obtaining accurate wind speed predictions is becoming more important for wind farm management. If the bias in wind speed prediction is reduced by 10%, the associated benefits gained from estimating power output rapidly increase in the electricity market [2]. Farm managers are obliged to predict wind speed, and the prediction of wind speed is a component of the overall wind farm management system. Thus, several studies have been conducted to improve the accuracy of wind speed predictions.

Currently, the MAPEs of wind speed predictions are between 25% and 40%. These values are affected by the prediction methods used as well as by the prediction horizon and wind speed characteristics at a given location [58]. In this study, a hybrid method that combined the SAM, ESM, and RBFN methods was proposed and tested with real wind speed datasets from two meteorological stations in the Hexi Corridor of China. The numerical results indicated that the MAPE values of the proposed approach were 12% and 16% for the two real wind speed datasets. In addition, the proposed approach was superior to the HWM, MLP, ESM, RBFN, SAM–ESM, SAM–RBFN, and ESM–RBFN approaches. Relative to the range of 25–40%, the prediction accuracy of the proposed method increased by approximately 10%. In addition, the associated benefits for estimating the predicted power output were rapidly increased. The proposed approach was effective in improving the prediction accuracy. In addition, this approach will likely benefit trading in the electricity market.

However, limitations exist despite the effectiveness of the hybrid model. For example, only the hourly wind speed data were used as an example to evaluate the performances of the proposed approaches in this study. Because the hourly data only reflect the short-term wind speed patterns, the predictions generated from these results provide useful information only for short-term predictions and decision-making. Thus, a hybrid model for predicting monthly or quarterly wind speed data could be created to improve this model. In addition, other prediction tools could be combined to improve these time-series predictions.

Acknowledgments

This research was supported by the National Basic Research Program of China '973' Program (Grant No. 2012CB956200) and the Opening Fund of Key Laboratory for Land Surface Process and Climate Change in Cold and Arid Regions, Chinese Academy of Sciences (No. LPCC201201). In addition, the authors also thank the editor, associate editor, and five anonymous referees for their valuable comments that greatly improved the quality of this paper.

References

[1] R. Ata, Y. Kocyigit, An adaptive neuro-fuzzy inference system approach for prediction of tip speed ratio in wind turbines, Expert Syst. Appl. 37 (2010) 5454–5460.
[2] R.J. Barthelmie, F. Murray, S.C. Pryor, The economic benefit of short-term forecasting for wind energy in the UK electricity market, Energy Policy 36 (2008) 1687–1696.
[3] C. Bishop, Improving the generalization properties of radial basis function neural networks, Neural Comput. 3 (1991) 579–588.
[4] Y. Bodyanskiy, O. Vynokurova, Hybrid adaptive wavelet-neuro-fuzzy system for chaotic time series identification, Inf. Sci. 220 (2013) 170–179.
[5] G.E.P. Box, G.M. Jenkins, G.C. Reinsel, Time Series Analysis: Forecasting and Control, fourth ed., John Wiley & Sons, Inc, Hoboken, New Jersey, 2008.
[6] E. Cadenas, O.A. Jaramillo, W. Rivera, Analysis and forecasting of wind velocity in Chetumal, Quintana Roo, using the single exponential smoothing method, Renew. Energy 35 (2010) 925–930.
[7] E. Cadenas, W. Rivera, Short term wind speed forecasting in La Venta, Oaxaca, México, using artificial neural networks, Renew. Energy 34 (2009) 274–278.
[8] C. Chatfield, What is the 'best' method of forecasting?, J Appl. Stat. 15 (1998) 19–39.
[9] K.W. Chau, Particle swarm optimization training algorithm for ANNs in stage prediction of Shing Mun River, J. Hydrol. 329 (2006) 363–367.
[10] M.Y. Chen, A hybrid ANFIS model for business failure prediction utilizing particle swarm optimization and subtractive clustering, Inf. Sci. 220 (2013) 180–195.

[11] S.M. Chen, P.Y. Kao, TAIEX forecasting based on fuzzy time series, particle swarm optimization techniques and support vector machines, Inf. Sci. 247 (2013) 62–71.
[12] C.T. Cheng, C.P. Ou, K.W. Chau, Combining a fuzzy optimal model with a genetic algorithm to solve multi-objective rainfall–runoff model calibration, J. Hydrol. 268 (2002) 72–86.
[13] F.X. Diebold, R.S. Mariano, Comparing predictive accuracy, J. Bus. Econ. Stat. 13 (1995) 253–263.
[14] E. Erdem, J. Shi, ARMA based approaches for forecasting the tuple of wind speed and direction, Appl. Energy 88 (2011) 1405–1414.
[15] C.X. Fan, S.Q. Liu, Wind speed forecasting method: gray related weighted combination with revised parameter, Energy Proc. 5 (2011) 550–554.
[16] M.H. Fazel Zarandi, M. Zarinbal, N. Ghanbari, I.B. Turksen, A new fuzzy functions model tuned by hybridizing imperialist competitive algorithm and simulated annealing application: stock price prediction, Inf. Sci. 222 (2013) 213–228.
[17] P. Flores, A. Tapia, G. Tapia, Application of a control algorithm for wind speed prediction and active power generation, Renew. Energy 30 (2005) 523–536.
[18] J.E.S. Gardner, Exponential smoothing: the state of art – Part II, Int. J. Forecast. 22 (2006) 637–666.
[19] S.L. Goh, M. Chen, D.H. Popovic, K. Aihara, D. Obradovic, D.P. Mandic, Complex-valued forecasting of wind profile, Renew. Energy 31 (2006) 1733–1750.
[20] Z.H. Guo, J. Wu, H.Y. Lu, J.Z. Wang, A case study on a hybrid wind speed forecasting method using BP neural network, Knowl.-Based Syst. 24 (2011) 1048–1056.
[21] Z.X. Guo, W.K. Wong, M. Li, Sparsely connected neural network-based time series forecasting, Inf. Sci. 193 (2012) 54–71.
[22] C. Hamzace, Improving artificial neural networks' performance in seasonal time series forecasting, Inf. Sci. 178 (2008) 4550–4559.
[23] G.B. Huang, P. Saratchandran, N. Sundararajan, An efficient sequential learning algorithm for growing and pruning RBF (GAP-RBF) networks, IEEE Trans. Syst. Man Cyber. 34 (2004) 2284–2292.
[24] T. Jaditz, L.A. Riddick, C.L. Sayers, Multivariate nonlinear forecasting using financial information to forecast the real sector, Macroecon. Dyn. 2 (1998) 369–382.
[25] G.M. Jenkins, Some practical aspects of forecasting in organizations, J. Forecast. 1 (1982) 3–21.
[26] S.A. Kalogirou, Artificial neural networks in renewable energy systems applications: a review, Renew. Sustain. Energy Rev. 5 (2001) 373–401.
[27] R.G. Kavasseri, K. Seetharaman, Day-ahead wind speed forecasting using f-ARIMA models, Renew. Energy 34 (2009) 1388–1393.
[28] Y.L. Lean, K.K. Lai, S.Y. Wang, Multistage RBF neural network ensemble learning for exchange rates forecasting, Neurocomputing 71 (2008) 3295–3302.
[29] C.C. Lee, Y.C. Chiang, C.Y. Shih, C.L. Tsai, Noisy time series prediction using M-estimator based robust radial basis function neural networks with growing and pruning techniques, Expert Syst. Appl. 36 (2009) 4717–4724.
[30] J.Y. Lin, C.T. Cheng, K.W. Chau, Using support vector machines for long-term discharge prediction, Hydrol. Sci. J. 51 (2006) 599–612.
[31] K.P. Lin, P.F. Pai, Y.M. Lu, P.T. Chang, Revenue forecasting using a least-squares support vector regression model in a fuzzy environment, Inf. Sci. 220 (2013) 196–209.
[32] C.J. Lu, T.S. Lee, C.C. Chiu, Financial time series forecasting using independent component analysis and support vector regression, Decis. Support Syst. 47 (2009) 115–125.
[33] L. Ma, S.Y. Luan, C.W. Jiang, H.L. Liu, Y. Zhang, A review on the forecasting of wind speed and generated power, Renew. Sustain. Energy Rev. 13 (2009) 915–920.
[34] M.C. Mabel, E. Fernández, Analysis of wind power generation and prediction using ANN: a case study, Renew. Energy 33 (2008) 986–992.
[35] C.A. Maia, M.M. Goncalves, Application of switched adaptive system to load forecasting, Electr. Power Syst. Res. 78 (2008) 721–727.
[36] M. Mohandes, T. Halawani, S. Rehman, A.A. Hussain, Support vector machines for wind speed prediction, Renew. Energy 29 (2004) 939–947.
[37] M. Monfared, H. Rastegar, H.M. Kojabadi, A new strategy for wind speed forecasting using artificial intelligent methods, Renew. Energy 34 (2009) 845–848.
[38] N. Muttil, K.W. Chau, Neural network and genetic programming for modeling coastal algal blooms, Int. J. Environ. Pollut. 28 (2006) 223–238.
[39] D.X. Niu, S.H. Cao, J.C. Lu, Load Forecasting Technology and its Applications, second ed., Electric Power Press of China, 2009.
[40] J.K. Ord, A.B. Koehler, R.D. Snyder, Estimation and prediction for a class of dynamic non-linear statistical models, J. Am. Stat. Assoc. 92 (1977) 1621–1629.
[41] P.F. Pai, C.S. Lin, A hybrid ARIMA and support vector machines model in stock price forecasting, Omega-Int. J. Manage. Sci. 33 (2005) 497–505. Omega.
[42] J. Park, I.W. Sandberg, Universal approximation using radial-basis-function networks, Neural Comput. 3 (1991) 246–257.
[43] A.P. Plumb, R.C. Rowe, P. York, M. Brown, Optimisation of the predictive ability of artificial neural network (ANN) models: a comparison of three ANN programs and four classes of training algorithm, Eur. J. Pharm. Sci. 25 (2005) 395–405.
[44] P. Poggi, M. Muselli, G. Notton, C. Cristofari, A. Louche, Forecasting and simulating wind speed in Corsica by using an autoregressive model, Energy Convers. Manage. 44 (2003) 3177–3196.
[45] T. Poggio, F. Girosi, Networks for approximation and learning, Proc. IEEE 78 (1990) 1481–1497.
[46] A.C. Pollock, A. Macaulay, M.E. Thomson, D. Onkal, Performance evaluation of judgemental directional exchange rate predictions, Int. J. Forecast. 21 (2005) 473–489.
[47] S.S. Sancho, M.P.B. Angel, G.O.G. Emilio, P.F. Antonio, P. Luis, C. Francisco, Accurate short-term wind speed prediction by exploiting diversity in input data using banks of artificial neural networks, Neurocomputing 72 (2009) 1336–1341.
[48] S.S. Sancho, G.O.G. Emilio, M.P.B. Ángel, P.F. Antonio, P. Luis, Short term wind speed prediction based on evolutionary support vector regression algorithms, Expert Syst. Appl. 38 (2011) 4052–4057.
[49] A. Sfetsos, A novel approach for the forecasting of mean hourly wind speed time series, Renew. Energy 27 (2002) 163–174.
[50] A. Sfetsos, A comparison of various forecasting techniques applied to mean hourly wind speed time series, Renew. Energy 21 (2000) 23–35.
[51] B.L. Smith, B.M. Williams, R.K. Oswald, Comparison of parametric and non-parametric models for traffic flow forecasting, Transp. Res. Part C 10 (2002) 303–321.
[52] N.D. Uri, Forecasting: a hybrid approach, Omega-Int. J. Manage. Sci. 5 (1977) 463–472.
[53] J.J. Wang, J.Z. Wang, Z.G. Zhang, S.P. Guo, Stock index forecasting based on a hybrid model, Omega-Int. J. Manage. Sci. 40 (2012) 758–766.
[54] D.K. Wedding, K.J. Cios, Time series forecasting by combining RBF networks certainty factors and the Box–Jenkins model, Neurocomputing 10 (1996) 149–168.
[55] C.L. Wu, K.W. Chau, Y.S. Li, Predicting monthly streamflow using data-driven models coupled with data-preprocessing techniques, Water Resour. Res. (2009), http://dx.doi.org/10.1029/2007WR006737.
[56] Q. Wu, R. Law, E. Wu, J.X. Lin, A hybrid-forecasting model reducing Gaussian noise based on the Gaussian support vector regression machine and chaotic particle swarm optimization, Inf. Sci. 238 (2013) 96–110.
[57] J.X. Xie, C.T. Cheng, K.W. Chau, Y.Z. Pei, A hybrid adaptive time-delay neural network model for multi-step-ahead prediction of sunspot activity, Int. J. Environ. Pollut. 28 (2006) 364–381.
[58] X. Yang, Y. Xiao, S. Chen, Wind speed and generated power forecasting in wind farm, Proc. CSEE 25 (2005) 1–5 (in Chinese).
[59] L. Yu, W. Huang, K.K. Lai, S.Y. Wang, A reliability-based RBF network ensemble model for foreign exchange rates prediction, in: I. King et al. (Eds.), ICONIP 2006, Part III, Lecture Notes in Computer Science, vol. 4234, 2006, pp. 380–389.
[60] G.P. Zhang, M. Qi, Neural network forecasting for seasonal and trend time series, Eur. J. Oper. Res. 160 (2005) 501–514.
[61] G. Zhang, Time series forecasting using a hybrid ARIMA and neural network model, Neurocomputing 50 (2003) 159–175.
[62] J.Y. Zhou, J. Shi, G. Li, Fine tuning support vector machines for short-term wind speed forecasting, Energy Convers. Manage. 52 (2011) 1990–1998.